STEM CELLS TRANSLATIONAL MEDICINE®

TISSUE ENGINEERING AND REGENERATIVE MEDICINE

Generation of a Functioning and Self-Renewing Diaphragmatic Muscle Construct

CATERINA TREVISAN,[a,b] MARIO ENRIQUE ALVREZ FALLAS,[a,b] EDOARDO MAGHIN,[a,b] CHIARA FRANZIN,[a] PIERO PAVAN,[a,c,d] PAOLA CACCIN,[e] ANGELA CHIAVEGATO,[e,f] EUGENIA CARRARO,[a] DANIELE BOSO,[a] FRANCESCO BOLDRIN,[g] FEDERICO CAICCI,[g] ENRICA BERTIN,[a] LUCA URBANI,[h,i,j] ANNA MILAN,[a,b] CARLO BIZ,[k] LORENZA LAZZARI,[l] PAOLO DE COPPI,[h,m] MICHELA POZZOBON,[a,b] MARTINA PICCOLI [a,e]

Key Words. Decellularized scaffold • Extracellular matrix • Diaphragm • Human muscle precursor cells • Recellularization

ABSTRACT

Surgical repair of large muscular defects requires the use of autologous graft transfer or prosthetic material. Naturally derived matrices are biocompatible materials obtained by tissue decellularization and are commonly used in clinical practice. Despite promising applications described in the literature, the use of acellular matrices to repair large defects has been only partially successful, highlighting the need for more efficient constructs. Scaffold recellularization by means of tissue engineering may improve not only the structure of the matrix, but also its ability to functionally interact with the host. The development of such a complex construct is challenging, due to the complexity of the native organ architecture and the difficulties in recreating the cellular niche with both proliferative and differentiating potential during growth or after damage. In this study, we tested a mouse decellularized diaphragmatic extracellular matrix (ECM) previously described by our group, for the generation of a cellular skeletal muscle construct with functional features. The decellularized matrix was stored using different conditions to mimic the off-the-shelf clinical need. Pediatric human muscle precursors were seeded into the decellularized scaffold, demonstrating proliferation and differentiation capability, giving rise to a functioning three-dimensional skeletal muscle structure. Furthermore, we exposed the engineered construct to cardiotoxin injury and demonstrated its ability to activate a regenerative response in vitro promoting cell self-renewal and a positive ECM remodeling. Functional reconstruction of an engineered skeletal muscle with maintenance of a stem cell pool makes this a promising tool toward future clinical applications in diaphragmatic regeneration. STEM CELLS TRANSLATIONAL MEDICINE *2019;00:1–12*

SIGNIFICANCE STATEMENT

In the present work, a storable and ready-to-use decellularized diaphragm-derived extracellular matrix (ECM) was used as cell support to generate a self-renewing skeletal muscle xenogeneic construct, as a combination of a mouse-derived ECM and human progenitor cells. This work represents a step forward toward the generation of tissue engineering xenograft for skeletal muscle clinical applications.

INTRODUCTION

Surgical treatment of a variety of pathological conditions, including malformations, congenital defects, post-traumatic muscle loss, and postsurgery tissue ablation, remains challenging. Conventional treatments involving primary repairs, autograft and free flaps, or prosthetic material have several limitations, including strength, growth, and susceptibility to infections [1–4]. On the other hand, skeletal muscle tissue regeneration has been widely investigated and different tissue engineering approaches have been used [5–8]. Tissue engineering aims to regenerate damaged tissue by recreating a microenvironment similar to the original. This purpose requires the right culture setting (e.g., oxygenation and mechanical stimuli), appropriate progenitor cells able to differentiate into the desired lineage and scaffolds that foster cell–matrix interaction and tissue regeneration. Up to now, tissue engineering has been successfully applied for the regeneration of several organs such as urinary bladder [9, 10], vagina [11], trachea [12], heart [13, 14], and skin [15]. Skeletal muscle is more challenging and the possibility of recreating alternative functional transplantable muscle that could be efficiently used for patients remains an unmet clinical need. Skeletal muscle

[a]Fondazione Istituto di Ricerca Pediatrica Città della Speranza, Padova, Italy; [b]Department of Women and Children Health, University of Padova, Padova, Italy; [c]Department of Industrial Engineering, University of Padova, Padova, Italy; [d]Centre for Mechanics of Biological Materials, University of Padova, Padova, Italy; [e]Department of Biomedical Sciences, University of Padova, Padova, Italy; [f]CNR Institute for Neuroscience, Padova, Italy; [g]Department of Biology, University of Padova, Padova, Italy; [h]Stem Cells & Regenerative Medicine Section, Developmental Biology & Cancer Programme, UCL Great Ormond Street Institute of Child Health, London, United Kingdom; [i]Institute of Hepatology, The Foundation for Liver Research, London, United Kingdom; [j]Faculty of Life Sciences & Medicine, King's College, London, United Kingdom; [k]Department of Surgery, Oncology, and Gastroenterology DiSCOG, Orthopaedic Clinic, University of Padova, Padua, Italy; [l]Laboratory of Regenerative Medicine – Cell Factory, Department of Transfusion Medicine and Hematology, Fondazione IRCCS Ca' Granda Ospedale Maggiore Policlinico, Milano, Italy; [m]Specialist Neonatal and Paediatric Surgery, Great Ormond Street Institute of Child Health, London, United Kingdom

Correspondence: Martina Piccoli, Ph.D., Tissue Engineering Lab, Istituto di Ricerca Pediatrica Città della Speranza, Corso Stati Uniti 4, 35129 Padova, Italy. Telephone: 39-049-9640129; e-mail: m.piccoli@irpcds.org; or Michela Pozzobon, Ph.D., Stem Cells and Regenerative Medicine Lab, Istituto di Ricerca Pediatrica Città della Speranza, Corso Stati Uniti 4, 35129 Padova, Italy. Telephone: 39-049-9640126; e-mail: m.pozzobon@irpcds.org

Received September 24, 2018; accepted for publication March 4, 2019.

http://dx.doi.org/10.1002/sctm.18-0206

is a finely organized tissue in which myofiber correct organization and coordination ensures muscle contraction and relaxation, thereby enabling tissue function. The thoracic diaphragm is a complex muscle organ essential to support respiration [16, 17]. The diaphragm also exerts nonrespiratory functions, including the promotion of venous return, lymphatic sieving, and gastroesophageal reflux restriction [18–22]. All these functions are supported by a unique anatomy: diaphragm is flat, with a central tendon and outward radiating myofibers [23]. Traumatic events or congenital defects (as congenital diaphragmatic hernia [CDH]) are phenomena that affect diaphragm integrity and functions, leading to the herniation of the abdominal organs into the thoracic cavity. In CDH, diaphragm defect size is one of the most important aspects in the choice of the appropriate approach to repair the hernia [24]. Primary repair is the preferred method but is not possible in larger defects. In such cases, a patch of polytetrafluoroethylene (PTFE) is usually applied [25]. However, reherniation occurs in 28%–50% of cases, generally around 12 months after implantation [26–28], compelling patients to undergo multiple surgeries and increasing risks and drawbacks. The use of biologically derived scaffolds for hernia repair such as acellular dermal matrix or intestinal submucosa, has been shown to be successful [29], but clinical study did not find a difference in the rate of recurrences between acellular matrix and PTFE [26].

Extracellular matrix (ECM) biologic scaffolds are usually derived via mammalian tissue decellularization, a process that removes cells while retaining the architecture and composition of the native ECM. This technique allows not only to avoid adverse antigenic response once decellularized ECM is implanted in vivo in allogenic settings, but also to promote the engraftment of seeded and host-derived invading cells [8, 30]. Recently, we extensively characterized the ECM obtained from decellularized mouse diaphragm and demonstrated the ability of this natural-derived scaffold to recruit host muscle precursor cells (MPCs) when orthotopically implanted in wild and atrophic mouse models [31]. This scaffold showed significant characteristics, such as the preservation of decellularized myofiber structure and composition, biomechanical features similar to native diaphragms, positive immunological properties, and angiogenic activity [32]. For these reasons, we believe that it can be considered an excellent candidate scaffold to support the in vitro generation of a diaphragmatic muscle construct.

In recreating an in vitro engineered tissue, the choice of the most appropriate cell source for scaffold recellularization is of paramount importance. The ideal cell population should be (a) derived from an easily accessible source, (b) capable of proliferation and self-renew, in order to guarantee a complete scaffold repopulation, and (c) able to differentiate giving rise to the cell types necessary for tissue function [33]. Human MPCs (hMPCs) are progenitor cells committed toward muscle lineage that can be easily isolated from small human muscle biopsies and hold the ability to grow in culture maintaining self-renewal and proliferation ability along with myogenic potential [34, 35]. Given their specificity and commitment, hMPCs have been chosen as cell source in several muscle tissue engineering studies [36, 37].

In the present work, we described a storage protocol for the long-term preservation of mouse decellularized diaphragm-derived ECM (dECM), which was then repopulated with pediatric hMPCs. Our proof of principle study was focused on the in vitro engineering and functional characterization of a construct for future diaphragmatic tissue regeneration. Finally, in order to prove the ability of self-renewing, we applied an injury to the xenograft and demonstrated its ability to activate a regeneration process that involves proliferation and differentiation of engrafted progenitor cells and also modification of the cellular niche.

Materials and Methods

Diaphragm Muscle Decellularization

Diaphragm muscles obtained from 3-month-old C57BL/6j mice (protocol number 1103/2016 approved by animal wellness local ethics committee Organismo per il Benessere Animale, Padova; all experiments were performed in accordance with relevant guidelines and regulations) were washed two times in 1× sterile phosphate-buffered saline (PBS, Gibco, Fisher Scientific, Monza, Italy) and then transferred in deionized water in order to start the decellularization process. Diaphragms were processed with three detergent-enzymatic treatment (DET) cycles in order to obtain a complete cell removal. Each DET cycle was composed of deionized water at 4°C for 24 hours, 4% sodium deoxycholate (Sigma, Merck KGaA, Darmstadt, Germany) at room temperature (RT) for 4 hours, and 2,000 kU DNase-I (Sigma, Merck KGaA, Darmstadt, Germany) in 1 M NaCl (Sigma, Merck KGaA, Darmstadt, Germany) at RT for 3 hours [31]. After decellularization, matrices were washed for at least 3 days in deionized sterile water and immediately analyzed or preserved in different storage conditions.

Diaphragm ECM Storage

Five different conditions were tested to find the best compromise between matrix preservation and longest storing period possible: fresh (dECM analyzed immediately after DET protocol, $n = 9$); 2w4C (dECM preserved for 2 weeks at 4°C in 1× PBS supplemented with 3% pen/strep, $n = 9$); 2m4C (dECM preserved for 2 months at 4°C in 1× PBS supplemented with 3% pen/strep, $n = 9$); 2wLN (dECM preserved for 2 weeks in liquid nitrogen in freezing medium, $n = 9$); 2mLN (dECM preserved for 2 months in liquid nitrogen in freezing medium, $n = 9$). In 2w4C and 2m4C conditions, 1× PBS supplemented with 3% of pen/strep was changed every 3 days in order to maintain antibiotic coverage; in 2wLN and 2mLN conditions, freezing medium was composed of 10% Dulbecco's modified Eagle's medium (DMEM) high glucose (4.5 g/l D-glucose, Gibco-Fisher Scientific), 20% dimethyl sulfoxide (DMSO, Sigma–Aldrich), and 70% fetal bovine serum (FBS, Gibco-Fisher Scientific). Specifically, dECM were immersed in 1 ml of freezing medium, slowly cooled in cryoboxes overnight, and then transferred to liquid nitrogen. Stored dECM were defrosted the day before performing experiment, washed in 1× PBS supplemented with 3% pen/strep and preserved at 4°C for up to 12 hours.

Diaphragm ECM Components Quantifications

Wet samples for quantification were snap frozen before use. Collagen, sulfated glycosaminoglycan (sGAG), and elastin content on decellularized diaphragms were quantified using, respectively, the Sircol™ Collagen Assay, Blyscan GAG Assay Kit, and Fastin Elastin Assay Kit (all from Biocolor, Carrickfergus, United Kingdom) under manufacturer's instruction.

Histology and Immunofluorescence

Tissue samples were fixed in 4% paraformaldehyde (PFA, Sigma–Aldrich) for 1 hour at 4°C. Histology was evaluated using frozen sections (8–10 μm thick), stained with hematoxylin and eosin kit for rapid frozen sections, Masson's Trichrome (MT) with aniline blue kit or Alcian blue pH 2.5 kit (all from Bio-Optica, Milan, Italy) under manufacturer's instruction. For immunofluorescence analyses, sections were incubated with primary antibodies (1 hour at 37°C or overnight at 4°C), washed, and then incubated for 1 hour at 37°C with labeled Alexa Fluor secondary antibodies, as listed in Supporting Information Table S1. Finally, nuclei were counterstained with fluorescent mounting medium plus 100 ng/ml 4′,6-diamidino-2-phenylindole (Sigma–Aldrich). For each diaphragm, random pictures were collected with an inverted microscope.

Transmission Electron Microscopy

Samples for transmission electron microscopy were fixed in 4% PFA for 1 hour and then with 0.25% glutaraldehyde (Sigma–Aldrich) in 0.1 M sodium cacodylate buffer overnight. After wash, small portions were postfixed in osmium tetroxide 1% for 1 hour at 4°C and then embedded in Epon 812 resin. Ultrathin sections, obtained with a Reichert-Jung Ultracut ultramicrotome, were recovered on slot grids and counterstained with uranyl acetate and lead citrate. The samples were examined with a FEI Tecnai G2 transmission electron microscope operating at 100 kV. Images were captured with a Veleta (Olympus soft Imaging System, Segrate, Milan, Italy) digital camera.

Human Pediatric MPCs Isolation, Expansion, and Cell Cycle Length Estimation

Skeletal muscle samples were obtained from Pediatric Surgery Clinic (Azienda Ospedialiera di Padova, Padua, Italy) and Orthopedic Clinic, University of Padova (Padova, Italy). Patient tissues were collected after written informed consent following the protocols number 2682P and number 3030P, approved by Local Ethics Committee (Comitato etico per la sperimentazione clinica dell'Azienda Ospedaliera di Padova). From muscle biopsies, cells were isolated using a previously described protocol [34]. Briefly, the samples ($n = 7$) were minced in small pieces (1–2 mm^3) and incubated with 3 ml of 0.2% (wt/vol) collagenase I for 90 minutes at 37°C. The reaction was stopped by adding washing medium (DMEM low glucose, 20% FBS, 1% P/S) and the samples were then centrifuged and incubated in 2 ml of 0.05% trypsin–EDTA for 60 minutes at 37°C. Washing medium was added to stop the reaction and the cell suspension was filtered first through 70 μm and then 40 μm cell strainers. After centrifugation, 3 ml of lysis buffer was added for 5 minutes to lyse red blood cells and then stopped with washing medium. The cell suspension was centrifuged and the pellet was resuspended in proliferative medium (PM) in a well of a 6-wells culture plate. PM is composed of DMEM low glucose (1 g/l D-glucose, Gibco-Fisher Scientific) with 20% FBS, 10^{-6} M dexamethasone (Sigma–Aldrich), 10 ng/ml bFGF (R&D System, Minnesota, United States), 10 μg/ml insulin (Humulin Eli Lilly, Indiana, United States), and 1% pen/strep. During expansion, hMPCs were cultured in PM and kept at 37°C, 5% CO_2 with an oxygen tension of 20% in a humidified incubator. For myogenic differentiation, hMPCs at confluence were cultured for 96 hours in 24-wells tissue culture plates in fusion medium (FM), composed of α MEM (Gibco-Fisher Scientific) supplemented with 2% HS, 10 μg/ml insulin, and 1% pen/strep. For cell cycle length estimation, hMPCs isolated from three different biopsies were plated in a 24-wells plate and after 72 hours of culture the cell number was determined. Each sample was assessed in triplicate. Cycle length was estimated using the following Equation 1:

$$g = 72h \times \frac{\log 2}{\log (N72h/N0h)} \quad (1)$$

in which g is the generation time during the logarithmic phase of the growth curve, $N72\,h$ is the cell number at 72 hours and $N0\,h$ is the cell number at time 0 [38].

Flow Cytometry Analysis and Immunofluorescence

Cell surface antigen expression was analyzed by flow cytometry on cells detached with trypsin–EDTA treatment at passages 3 and 5 ($n = 7$). The antibodies used were: CD34 FITC, CD56 PE (both from BD Bioscience, Milan, Italy), 7-aminoactinomycinD was used as viability assay.

For immunofluorescence, both proliferating and differentiated cells from three different samples at passage 5 were incubated for 1 hour at 37°C with labeled Alexa Fluor secondary antibodies, as listed in Supporting Information Table S1. Nuclei were counterstained with HOECHST (Life Technologies, Thermo Fisher, Milan, Italy, dilution 1:10,000). To quantify myoblast fusion, the myogenic index (MI), defined as the number of nuclei residing in $MYHC^+$ cells containing three or more nuclei divided by the total number of nuclei, was calculated from five random fields of each sample [39].

Diaphragm ECM Recellularization

Mouse dECM stored in different conditions were used for the recellularization procedure. We performed $n = 7$ total experiments, $n = 5$ with fresh or 2w4C stored samples, and $n = 2$ with 2mLN stored diaphragms (this last condition is showed in Supporting Information Fig. S1). Decellularized diaphragms were divided in four patches of approximately 35 mm^2 (excluding the crural muscle). Each one was fixed with four little pins on a rubber support and placed into a well of a 6-wells plate. Human MPCs, previously expanded for 5 or 6 passages, were resuspended in 15 μl of human cord blood platelet gel supernatant (PGS) [40] and injected into the dECM at a density of 5×10^5 cells per patch. Decellularized diaphragms were used as controls. After 2 hours from the seeding, 8 ml of PM were added to each well, in order to completely cover the scaffolds. The PM was maintained for 4 days, then changed every other day before being replaced by FM, which was kept until the last experimental day. The cultures were analyzed after 4, 7, 12, or 21 days.

Evans Blue Injection

Thirty microliters of Evans blue dye (Sigma) were injected into a decellularized hemi-diaphragm fixed on a rubber support using a 33G needle Hamilton syringe, as shown in Supporting Information Movie S2. This procedure was used in pilot experiments to verify the injection efficiency.

Picogreen Assay

Recellularized samples were collected and immediately frozen in liquid nitrogen, then transferred at −80°C at least for 48 hours. Decellularized scaffolds were used as negative control and cells cultured on plastic as positive control. Samples were digested in a Proteinase K solution in phosphate buffer saline (PBS) buffer. PBS buffer was composed of: 20 mM Na_2HPO_4, 30 mM NaH_2PO_4 monohydrate, 5 mM Na_2EDTA in deionized water; the pH was

adjusted at 7.1 and the solution was then sterilized in autoclave at 121°C for 15 minutes. Proteinase K (Invitrogen, Thermo Fisher, Milan, Italy) was diluted in PBS buffer at the final concentration of 0.5 mg/ml. Each sample was immerged in 300 µl of digestion solution and incubated at 65°C overnight. Once the samples were completely digested, they were transferred into a black 96 wells-plate (Nunc MicroWell 96-Well Optical-Bottom Plates with Polymer Base, nontreated, Nunc, Thermo Fisher, Mila, Italy), and the DNA was quantified using Quant-iT PicoGreen dsDNA Assay Kit (Invitrogen), under manufacturer's instruction. The standard solution provided by the kit was used to create the standard curve. The fluorescent signal corresponding to the DNA amount was detected using VICTOR2 1420 Multilabel Counter (Perkin Elmer, Massachusetts, United States). Excitation $\lambda = 485$ nm and emission $\lambda = 535$ nm.

Western Blot

Decellularized and recellularized mouse dECM, fresh diaphragm, and hMPCs were solubilized in 1 ml of T-PER Tissue Protein Extraction Reagent (Thermo Fisher Scientific) and homogenized using TissueLyser (Qiagen, Hilden, Germany), according to manufacturer instructions. Then, equal amounts of protein extracts (25 µg) were resolved by SDS-PAGE gels (4%–12%, 3%–8%) and transferred to nitrocellulose transfer membrane (Advansta, California, United State). Membranes were blocked with Blotto nonfat dry milk (Santa Cruz, California, United State) for at least 1 hour at RT and then incubated overnight at 4°C under constant shaking with primary antibodies listed in Supporting Information Table S1. Membranes were next incubated with peroxidase-labeled secondary antibodies (Supporting Information Table S1), visualized using ECL Select, and exposed to Amersham Hyperfilm ECL (GE Healthcare, Milan, Italy).

Calcium Transient Assay

Recellularized samples of dECM or human MPC cells plated on 13 mm coverslips were loaded with 20 µM Fluo4_AM (Thermo Fisher Scientific) by incubation at 37°C for 30 minutes in Optimem Medium (Life Technologies) containing 0.04% Pluronic F-127 (Merck KGaA, Darmstadt, Germany), and washed with medium. Loaded samples were transferred under a TCS-SP5-RS confocal microscope (Leica, Wetzlar, Germany) equipped with a 20× objective (NA, 1.0). Laser emission at 488 nm was used for stimulation and emitted cell fluorescence at 530 nm was acquired, as basal value. Time frame acquisition of 491 milliseconds was used. Samples were then chemically stimulated with freshly prepared solution of ATP (1 mM), and emitted fluorescence acquired to record transient alteration in cytosolic calcium levels.

Cardiotoxin Injury of Recellularized ECM

Cardiotoxin (Ctx, Latoxan, Portes-lés-Valence, France), a snake venom commonly used in vitro and in vivo to damage skeletal muscle myofibers and initiate a regeneration process, was used to induce an injury on recellularized dECM. For these samples, 0.2 µM Ctx was added to the FM after 7 days of culture and it was maintained for 6 hours [41]. Then samples were either immediately fixed and analyzed or maintained for 5 days in PM and then analyzed.

RNA Extraction and Real Time PCR

Total RNA was extracted using RNeasy Plus Mini kit (Qiagen) following the supplier's instructions. RNA was quantified with a ND-2000 spectrophotometer and 1 µg was reverse transcripted with SuperScript II and related products (all from Life Technologies), in a 20 µl reaction. Real-time Polymerase Chain Reaction (PCR) reactions were performed using a LightCycler II (Roche, Basilea, Svizzerland). Reactions have been carried out in duplicate using Platinum SYBR Green qPCR SuperMix-UDG (Invitrogen) and 2 µl of primers mix FW + REV (final concentration, 300/300 nM) in a final volume of 20 µl. Serial dilutions of a positive control sample were used to create a standard curve for the relative quantification. The amount of each mRNA has been normalized for the content in *β2-microglobulin.* Primer sequences are listed in Supporting Information Table S2.

Statistical Analyses

Data are expressed as mean ± SEM. For immunofluorescence and histological analyses, at least 15 random high-power field areas were considered per analyzed muscle. Statistical significance was determined using a nonparametric Kruskal–Wallis test to analyze the variance followed by Dunn's multiple comparison test to estimate the statistical difference between each couple of groups. A *p*-value below .05 was considered statistically significant. The data that support the findings of this study are available from the corresponding author upon reasonable request.

RESULTS

dECM Scaffold Characterization at Different Storage Conditions

After decellularization, dECM scaffolds were stored for 2 weeks or 2 months in classic buffer (1× PBS + 3% pen/strep) at 4°C (2w4C and 2m4C, respectively; $n = 9$ for both conditions), or alternatively in liquid nitrogen (2wLN and 2mLN, $n = 9$ for both conditions) after a slow-cooling protocol using DMSO as cryoprotectant. Histological analysis was performed in order to examine the dECM integrity after each storing condition (Fig. 1A). The 2m4C condition was the worst in terms of ECM integrity preservation, as denucleated myofibers appeared desiccated and ruined, with an important loss of muscle fiber structure and content. For this reason, this experimental condition was excluded from subsequent analyses together with 2wLN, that resulted macroscopically well-preserved but, beside 2w4C storage, is less convenient and more expensive.

ECM component quantifications demonstrated that elastin and collagen content was preserved in the stored samples, even though longer stored scaffolds displayed a trend of increase in collagen per milligrams of wet tissue, possibly due to minimal collagen crystallization during storage and subsequently increased solubility (Fig. 1B, 1C). Although no significant difference was detected in sulfated GAG (sGAG) content in the two storing conditions, long-term storage in liquid nitrogen (2mLN) showed lower sGAG levels compared with freshly decellularized dECM (Fig. 1D). The overall result of these analyses showed no difference in dECM components between the two storage methods, but given the faster and cheaper preservation, 2w4C stored samples were used for successive recellulrization experiments. Also, electron microscopy analysis confirmed the occurred decellularization and the good maintenance of myofiber's structure after this type of storage (Supporting Information Fig. S1A); 2mLN samples were used to verify that recellularization is efficient and not impaired by a longer storage.

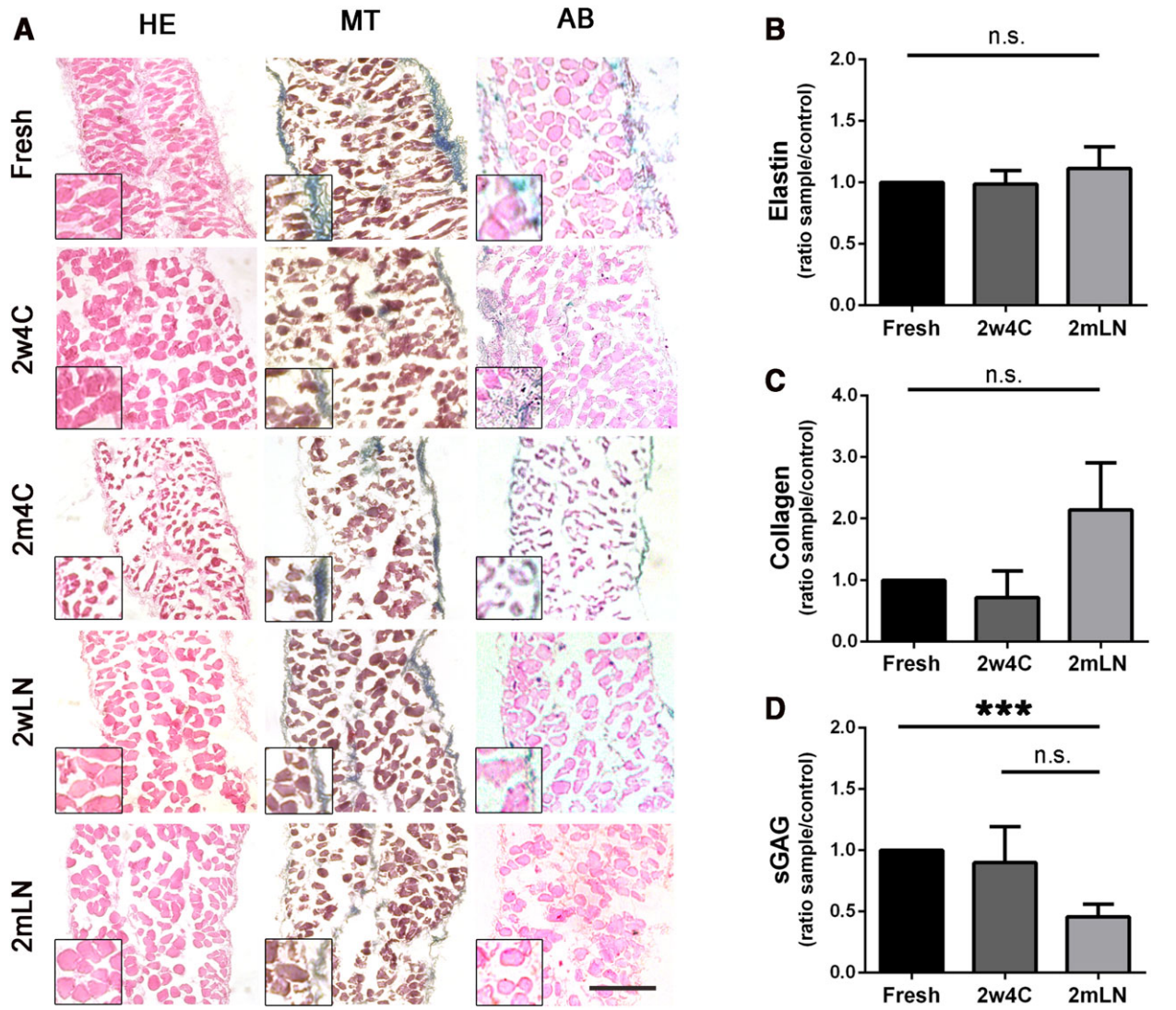

Figure 1. Characterization of stored and not stored (fresh) mouse decellularized diaphragms. **(A):** Histological analyses of diaphragmatic acellular scaffolds immediately after decellularization (fresh) or after different types and timings of storing: 2 weeks at 4°C (2w4C), 2 months at 4°C (2m4C), 2 weeks in liquid nitrogen (2wLN), and 2 months in liquid nitrogen (2mLN). HE stain for general appearance of the muscle, MT for collagen, AB for GAG. Scale bar: 100 µm. **(B–D):** Elastin, collagen, and sGAG quantifications of decellularized diaphragms. Fresh decellularized samples were used as control. ***, $p < .001$. Scale bar: 100 µm. Abbreviations: HE, hematoxylin and eosin; MT, Masson's trichrome; AB, Alcian blue; GAG, glycosaminoglycans; sGAG, sulfated GAG; n.s., not significant by Student's *t* test.

Human Pediatric MPC Isolation and Characterization

Similar to what we have previously demonstrated from adult healthy muscle biopsies [34], pediatric hMPCs were isolated and characterized in vitro for proliferative and differentiation abilities. After isolation, cells were expanded until passage 5 (Fig. 2A, 2B) in order to obtain a suitable number of cells for recellularization experiments (between 5 and 7 million cells within 3 weeks of culture), and then analyzed for the expression of the specific hMPC marker CD56 [34, 42, 43]. Only samples with at least 85% of $CD56^+$ cells were used in recellularization experiments (Fig. 2B). We estimated the cell cycle length of the culture (i.e., doubling time, 27.19 hours ± 4.88 hours; Fig. 2C) and the expression of the marker KI67 (52.62% ± 4.52%) in order to evaluate the cell proliferation in vitro (Fig. 2D, 2E). In addition, cells expressing the myogenic markers PAX7 (21.50% ± 2.26%), MYF5 (64.02% ± 2.51%), and MYOD (52.68% ± 3.08%) were quantified to better define the skeletal muscle phenotype, commitment, and regenerative potential of the isolated population (Fig. 2D, 2E). Cell differentiation ability was assessed after induction of cell fusion, by staining for myosin heavy chain (MYHC) and calculating the MI (0.51 ± 0.02), which demonstrated the maintenance of the differentiation capacity also after expansion (Fig. 2F). Moreover, differentiated cells demonstrated to be functionally activated since they respond to ATP stimulus modulating calcium transients (Supporting Information Movie S1). Being based on whole muscle digestion, the isolation procedure gave rise to a heterogeneous cell population, composed of myogenic cells and fibroblasts, identified by the presence of $TE7^+$ cells (fibroblast marker, 22.50% ± 3.34%; Fig. 2E, 2G).

dECM Scaffold Recellularization and Device Characterization

For the in vitro muscle generation, mouse decellularized diaphragms were divided in four parts discarding crural muscles and obtaining patches (0.5 cm × 0.7 cm) of costal muscle only

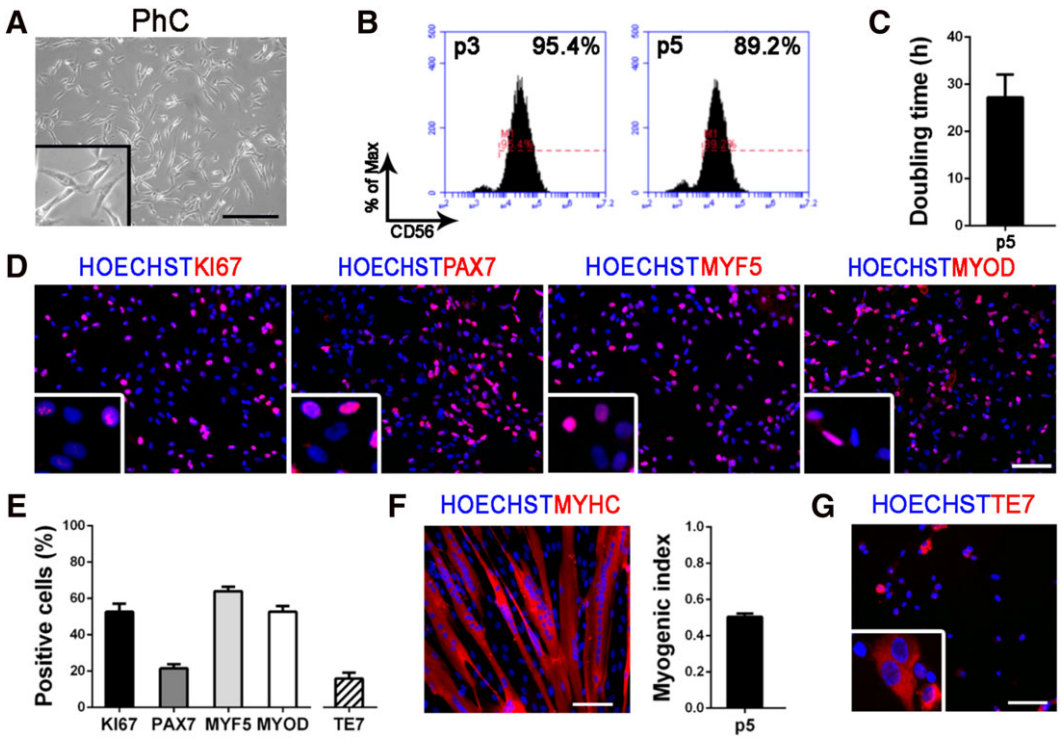

Figure 2. Characterization of pediatric human muscle precursor cells (hMPCs) at passage 5 (p5). **(A):** PhC image of pediatric hMPCs in vitro. **(B):** Histograms obtained from flow cytometry analyses and representing the percentage of $CD56^+$ cells (at p3 and p5). **(C):** Doubling time (hours) of pediatric hMPCs. **(D):** Immunofluorescence for KI67, PAX7, MYF5, and MYOD (in red); nuclei are counterstained with HOECHST (in blue). **(E):** Quantifications of $KI67^+$, $PAX7^+$, $MYF5^+$, $MYOD^+$, and $TE7^+$ cells. **(F):** Immunofluorescence after hMPCs differentiation. MYHC is shown in red and nuclei in blue (counterstained with HOECHST). Myogenic index of pediatric hMPCs in vitro at p5. **(G):** Immunofluorescence for TE7 (in red); nuclei are counterstained with HOECHST (in blue). All scale bars: 100 µm. Abbreviation: PhC, phase contrast.

(Fig. 3A). The scaffolds were mounted on a rubber support with pins, in order to both secure the dECM and stimulate a directional tension (Fig. 3B, 3D). Pilot experiments were done using Evans blue dye instead of a cell suspension, to experience injection efficiency (Supporting Information Fig. S2 and Supporting Information Movie S2). For recellularization experiments, pediatric hMPCs were collected, resuspended in PGS, and injected with a 33G needle into the dECM (Fig. 3C, 3D). PGS [40] was chosen as cell vehicle because of its richness in cytokines and growth factors [44, 45]. Recellularized scaffolds were analyzed after 4, 7, and 12 days of in vitro 3D culture. Human MPCs were able to engraft, as demonstrated by histology, immunofluorescence images (Fig. 3E, 3G and Supporting Information Fig. S3), and by DNA amount quantified through Picogreen assay (Fig. 3E, 3H). Comparable amount of DNA was detected after 7 days in culture in respect to a fresh control diaphragm (Fig. 3H). Interestingly, a homogeneous recellularization pattern was achieved also using 2mLN cryopreserved scaffolds (Supporting Information Fig. S4).

Human MPCs showed a tendency to maintain a similar cell density among 4, 7, and 12 days after seeding (Fig. 3I). As underlined by MT and fibronectin stains (Fig. 3E, 3G and Supporting Information Fig. S3), seeded cells were able to integrate within the scaffold, but also to actively secrete ECM components identified by fibronectin around cells. This ECM deposition, easily observed also by electron microscopy (Supporting Information Fig. S3B), together with the area populated by the injected cells, was likely to be responsible for the gradual increment of the scaffold thickness from day 4 to day 12 (Fig. 3K). Importantly, we calculated the cell distribution as the mean distance of farthest nuclei on the total scaffold thickness, and obtained an increase from 60% at 4 days to more than 80% at 12 days (Fig. 3J), with hMPCs able to colonize the scaffold both inserting between and infiltrating denucleated myofibers (Fig. 3L and Supporting Information Fig. S1B).

dECM Scaffold Allows hMPC Proliferation and Differentiation

Recellularized scaffolds were maintained in culture with PM for 4 days, then medium was changed to FM to stimulate cell differentiation and myotube formation, and PM was restored during the last 5 days of culture. According to this protocol, the highest percentage of $KI67^+$ proliferating cells was found after 4 days (10.20% ± 1.33%), and then decreased in the later time points (1.52% ± 0.51% at 7 days; 3.63% ± 0.48% at 12 days; Fig. 4A), confirming that seeded cells were able to respond microenvironment conditions. The number of $PAX7^+$ cells remained similar among all the time points even after stimulation by FM (18.99% ± 3.11% at 4 days; 16.70% ± 1.87% at 7 days; 16.62% ± 2.18% at 12 days), suggesting the maintenance of stem cell pool in the construct (Fig. 4B). Myogenic progenitor cell marker MYF5 was higher in the first time point compared with 7 and 12 days of culture (Fig. 4C). On the contrary, the expression of the differentiation marker α-sarcomeric actin (ACTA), increased from day 4 to day 12, confirming that also the differentiation commitment was efficiently reproduced in the engineered system (Fig. 4D and Supporting Information Fig. S3). In addition, early and late myogenic markers were investigated by real time PCR: as expected, *MYF5* and *MYOD* were highly expressed and continuously raised during the culture, highlighting the presence of a proliferating, and early differentiating myogenic

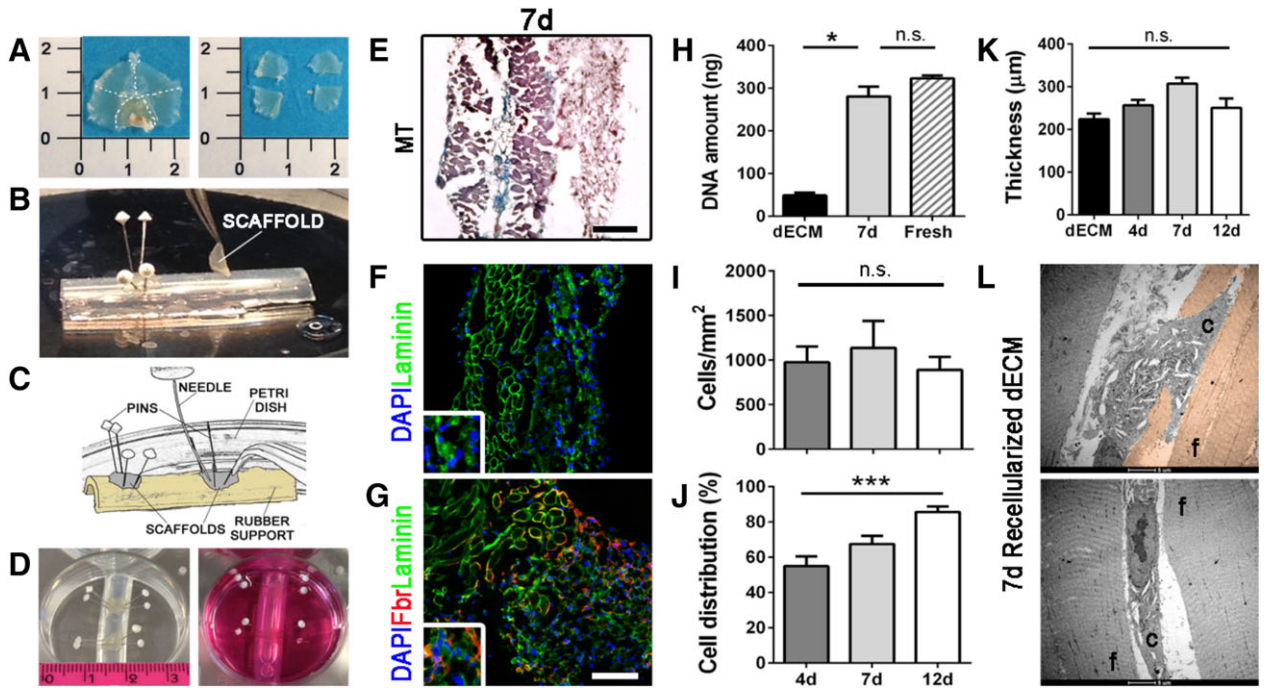

Figure 3. Recellularization procedure and characterization of recellularized diaphragmatic scaffolds. **(A):** Left: entire decellularized diaphragm. Right: four sections (50 mm^2 each) obtained from the entire decellularized diaphragm after the removal of the crural muscle. **(B):** Positioning of the decellularized scaffolds on the rubber support. The scaffolds were fixed with four pins following the fibers orientation. **(C):** Representative image describing the injection procedure. **(D):** Left: positioning of the rubber support with recellularized scaffolds on a well of a 6-wells plate. Right: medium addition. **(E):** Masson's trichrome staining for recellularized diaphragms after 7 days of culture. **(F):** Immunofluorescence of the recellularized samples showing hMPCs engraftment. Laminin (green) and nuclei counterstained with DAPI (blue). **(G):** Immunofluorescence of laminin and fibronectin (red). Nuclei were counterstained with DAPI. Scale bars: 100 μm. **(H):** DNA amount before (dECM) and after (7d) recellularization calculated with Picogreen assay. **(I):** Recellularized scaffold cell density (cells per mm^2) at different time points (cell density was calculated dividing the number of cells for the area of the diaphragm). **(J):** Cell distribution on recellularized samples. Hundred percentage is the full thickness of the decellularized scaffold. **(K):** Scaffold thickness before recellularization (dECM) and after 4, 7, and 12 days of culture from cell injection. **(L):** Electron microscopy of recellularized scaffold after 7 days in culture. Upper image: myogenic cell infiltrating an old de-nucleated fiber; lower image: myogenic cell inserting between two adjacent decellularized fibers. *, $p < .05$; **, $p < .01$. Abbreviations: C, cell; dECM, diaphragm-derived extracellular matrix; f, fiber; hMPCs, human muscle precursor cells; n.s., not significant by Student's *t* test.

population (Fig. 4E). Late differentiation markers *MYHC* and *DYSTROPHIN* (*DYSTR*) were more expressed at day 7 and 12 compared with day 4 (Fig. 4F). Mature skeletal muscle proteins were also investigated through Western blot, demonstrating the presence of both newly formed (MYH3) and mature (MYHC) myofibers inside the recellularized dECM after 7 days in culture (Fig. 4G). Given the strong expression of functional skeletal muscle markers, we investigated the maturity of regenerated myofibers inside the construct by analyzing calcium transient. Starting from 7 days of in vitro culture, our device showed to possess functioning myotubes able to answer to ATP stimulation with a fast and synchronous transient in cytosolic calcium concentration (Fig. 4H and Supporting Information Movie S3). All these results demonstrated that hMPCs were able to grow and functionally differentiate when seeded in a decellularized skeletal muscle tissue maintaining an intact stem cell pool at the same time.

The Construct Responds to Cardiotoxin Injury

To test the device regeneration potential in vitro, we damaged the construct with Ctx at 7 days of culture and analyzed its response 6 hours and 5 days after injury. The aim was to investigate the ability of the population of $PAX7^+$ cells to be activated and regenerate the damaged tissue as it happens physiologically in vivo. After injury, we found an increase of $KI67^+$ cells (threefold) only 5 days after injury (Fig. 5A), whereas at both 6 hours and 5 days, $PAX7^+$ cells raised in respect to uninjured control (3.4-fold and 4.4-fold, respectively; Fig. 5B). Interestingly, cells coexpressing PAX7 and KI67 were found greatly increased 5 days after injury (14-fold more than uninjured samples, Fig. 5C, 5D), confirming the presence of a functional stem cell pool preserving physiological features inside the construct. These results were confirmed also by molecular biology analyses in which we found an overexpression of *PAX7* and *MYF5* transcripts 5 days after Ctx injury in respect to 6 hours injured samples and 7 days uninjured control (Fig. 5D). Moreover, 5 days after injury, the graft was able to regenerate and to produce new skeletal muscle tissue since we found a regain of *MYHC* gene expression and several MYHC and ACTA positive myotubes (Fig. 5E, 5F). Also *LAMA1*, a gene responsible of stem cell niche reconstitution and basal lamina production after damage was overexpressed after Ctx injury in respect to 7-days uninjured control, and its upregulation gradually decreased during the days following the injury (Fig. 5G), as described in the literature [46]. Together with production of new basal lamina components, regenerating satellite cells are able to transiently remodel their niche producing the ECM glycoprotein fibronectin [47]. In our device, 5 days after Ctx injury there was an increased production of fibronectin (Fig. 5G), confirming the

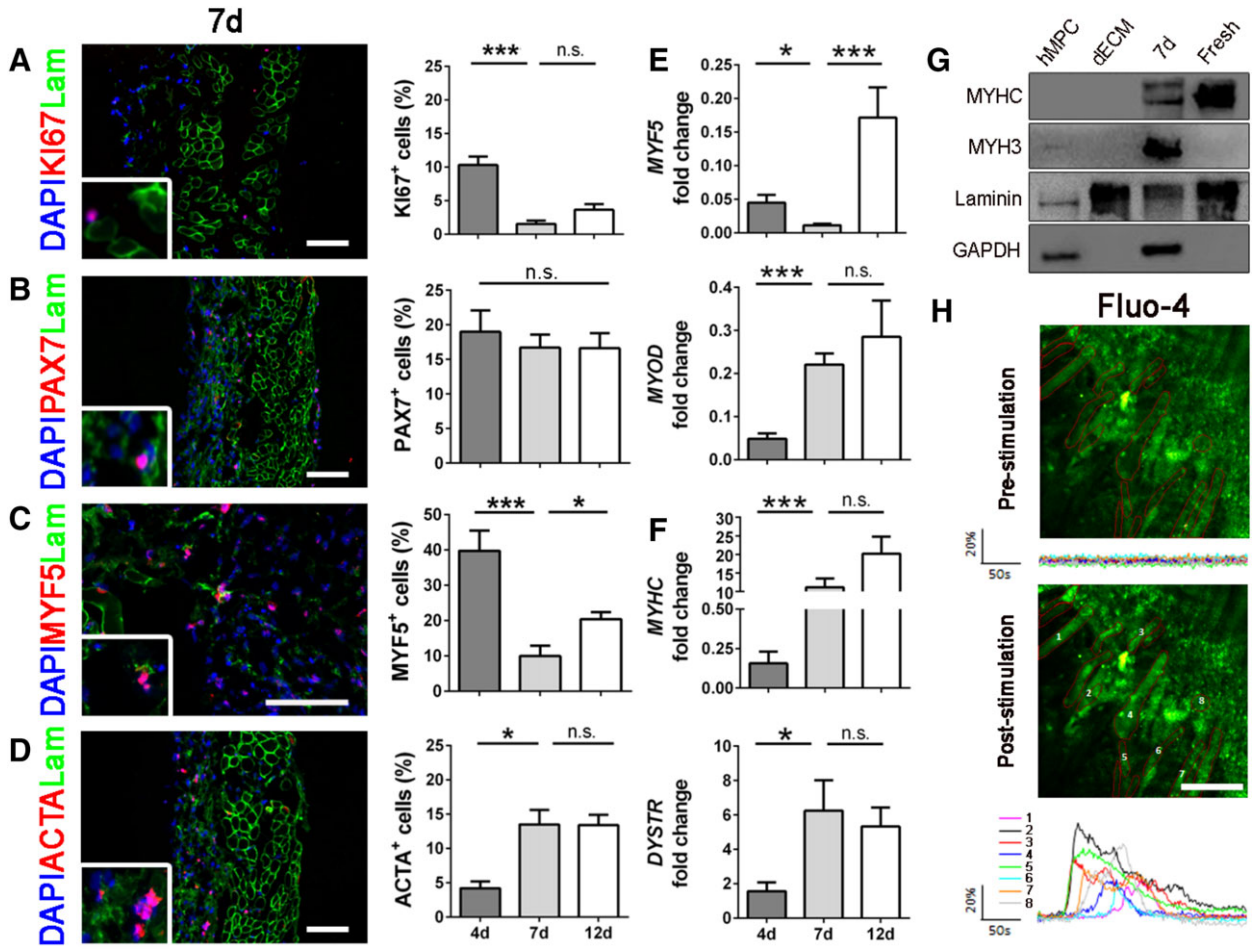

Figure 4. Immunofluorescence, quantifications, and molecular biology analyses of early and late myogenic markers. **(A):** Representative immunofluorescence images of recellularized samples after 7 days. KI67 (red), laminin (green), and nuclei counterstained with DAPI (blue). Quantifications were done at days 4, 7, and 12. **(B):** Immunofluorescence of satellite cells marker PAX7 (red) and related quantifications. **(C):** Immunofluorescence and quantifications of the early myogenic marker MYF5 (red). **(D):** Immunofluorescence and quantification of the late myogenic marker ACTA (red). **(E):** Molecular biology analyses (real time PCR) at 4, 7, and 12 days of early myogenic markers *MYF5* and *MYOD*. **(F):** Molecular biology analyses of late myogenic markers *MYHC* and *DYSTR*. **(G):** Western blot analyses of mature myogenic proteins. GAPDH was used as human specific cell marker, laminin as extracellular matrix control. **(H):** Representative images of recellularized samples after 7 days in culture with myotubes loaded with the calcium dye Fluo-4 AM and stimulated by ATP application. Graphics show mean fluorescence intensity (ΔF/F0) of the Region of Interests depicted. All scale bars: 100 μm. *, $p < .05$; **, $p < .01$; ***, $p < .001$; n.s., not significant by Mann–Whitney *U* test.

ability of engrafted PAX7$^+$ cells to regenerate the muscle-like construct by modulating their behavior and environment.

To verify that the stem cell pool is maintained also in a more mature construct and that regeneration process is able to be activated distantly from the initial cell seeding, we decided to damage the construct with Ctx 21 days after recellularization, and to analyze the percentage of PAX7$^+$ cells 5 days after injury. In this longer time point, the construct expressed functional muscle proteins such as MYH3, Desmin, and Dystrophin (Supporting Information Fig. S5A) more strongly than after 7 and 12 days of culture. Interestingly, also in this mature construct, the percentage of PAX7$^+$ cells increased by the same fold (approximately 3) after Ctx treatment (Supporting Information Fig. S5B), emphasizing that the regenerative potential of engrafted stem cells remained unaltered when cultured on dECM.

Discussion

Engineering skeletal muscle for the therapy remains a challenge. In this work, we demonstrated the ability of hMPCs to repopulate a decellularized dECM scaffold and to generate in vitro a self-renewing device, as proof of principle for future preclinical and clinical studies. The aim was to identify the best technique to recreate in vitro diaphragmatic muscle tissues combining a natural derived-ECM and patient specific progenitor cells, in order to obtain possible substitutes for diaphragm muscle diseases.

When designing a construct to be used in a clinical setting, it is important to develop a feasible and effective storage method that allows the scaffold to be preserved in the manufacturing facility and made rapidly available to the clinicians as an off-the-shelf product. This is a critical step and would allow widening clinical applications of tissue engineered products to more emergency situations [12]. Despite the literature, several research papers reported the scaffold storage after lyophilization [48–50], our aim was to preserve dECM structure and architecture also after storage without the need for swelling procedure, to obtain in vitro a construct as similar as possible to the original muscle. Giving that dECM was preserved in a better condition when stored for a short

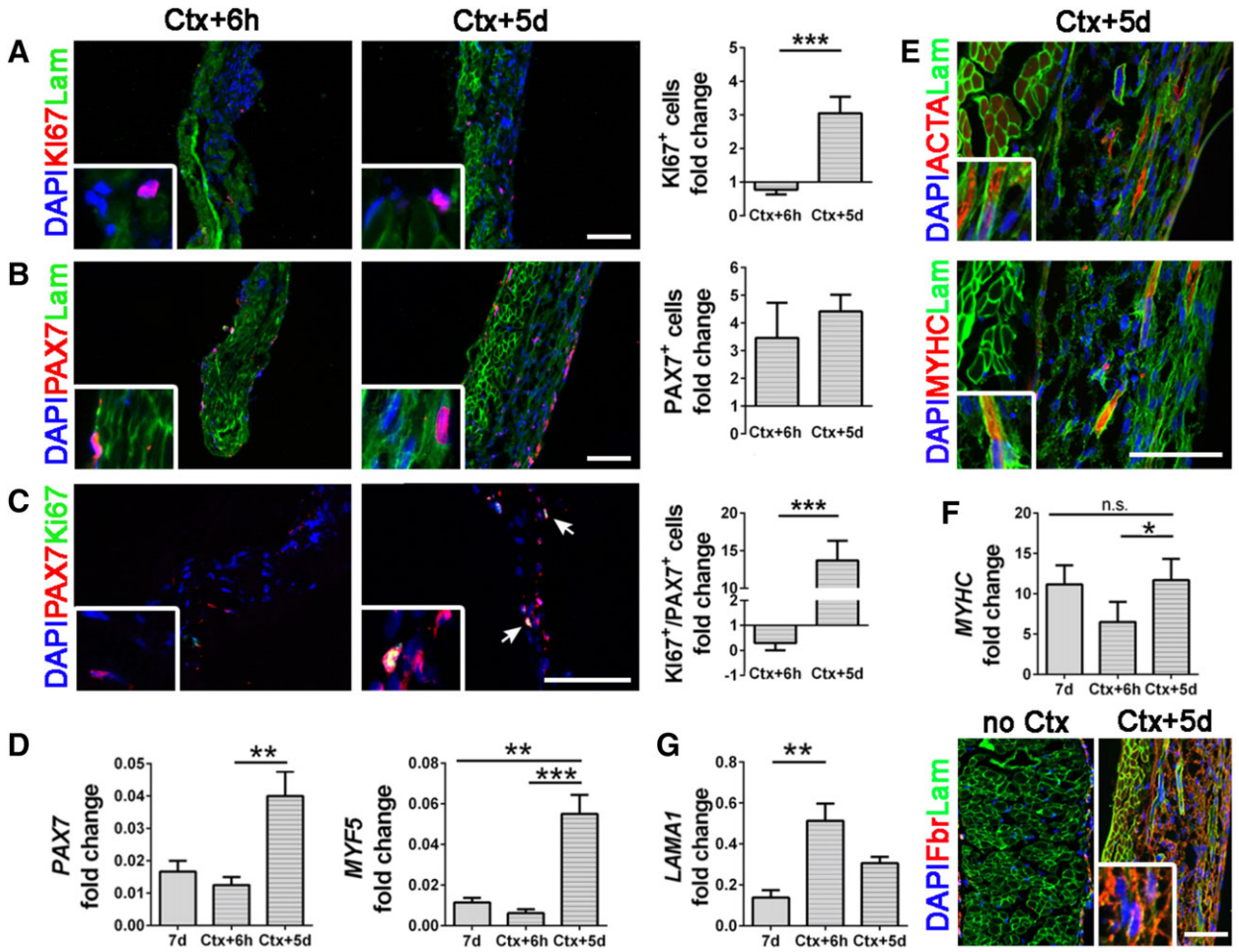

Figure 5. Characterization of recellularized samples after Ctx injury. **(A):** Immunofluorescence and quantifications of KI67$^+$ cells (red). Laminin (green) and nuclei counterstained with DAPI (blue). **(B):** Immunofluorescence images and quantifications for PAX7$^+$ cells (red). **(C):** Costaining for PAX7$^+$ (red) and KI67$^+$ (green) cells, nuclei colored with DAPI and related quantifications. Quantifications were normalized on noninjured 7 days samples. **(D):** Molecular biology analyses (real time PCR) of PAX7 and MYF5 at 7 days and 6 hours or 5 days after Ctx injury. **(E):** Representative immunofluorescence images of ACTA (on the top) and MYHC (on the bottom) for the Ctx + 5d sample. Laminin (green) and nuclei counterstained with DAPI. **(F):** Transcription of *MYHC* at 7 days and 6 hours or 5 days after Ctx injury. **(G):** Molecular biology analysis of *LAMA1* expression at 7 days and 6 hours or 5 days after Ctx injury and representative immunofluorescent image of fibronectin production in uninjured samples (no Ctx) and 5 days after Ctx injury. Laminin (green) and nuclei counterstained with DAPI. All scale bars: 100 μm. ***, $p < .001$.

period or using a cryoprotectant for longer time, as it happens for other biologic-derived scaffolds [51], it means that this product can be treated as a fresh and viable tissue, and that standard GMP storage rules could be applied also to dECM [52]. Nevertheless, the scaffolds used in this study were from rodents that, together with other important manufacturing issues (i.e., decontamination and sterilization), should be reconsidered before a possible clinical translation, possibly moving to the use of large animal model or human tissue samples [53].

We have previously described that decellularized dECM triggers myogenic cell activation and skeletal muscle regeneration when implanted in vivo, both in wild and atrophic mouse models [31]. Preclinical studies with in vivo application of decellularized matrices for skeletal muscle regeneration demonstrated a similar positive remodeling process, such as scaffold degradation by host cells, vascularization, and recruitment of stem/progenitor cells to the site of implantation [7, 8, 31, 54]. In previous studies, despite the presence of new muscle fibers in the treated area, none of the experiments succeeded in mimicking the precise organization of the native muscle [54–56]. This is probably due to the lack of specific signals toward regeneration inside the implanted dECM [57], especially when used to repair large muscle defects, an important aspect not only in the tissue regeneration after damage or loss of muscle volume, but also in the treatment of skeletal muscle congenital defects such as CDH. This limitation highlights the need for alternative scaffolds capable to boost myofiber generation to improve tissue functionality. Bioscaffolds engineered with cells are an option to overcome the limitations related to the use of acellular matrix alone [58], increasing ate the same time healing process and the better clinical outcome.

In this view, we were able to produce a viable and functional construct generated by the combination of animal-derived dECM and human muscle progenitor cells. Up to now, a variety of tissue engineering strategies have been described to develop 2D and 3D skeletal muscle constructs, employing variable scaffold materials and cell types [5, 41, 59–63]. Nevertheless, the in vitro generation of a skeletal muscle construct

with structural and functional characteristics comparable to the native tissue is still a major challenge. One of the most important features in the development of an engineered tissue is the choice of the best cell type. Cell sources for therapeutic implantation include embryonic stem cells (ESCs), induced-pluripotent stem cells (iPSCs), fetal, and adult muscle stem cells, as well as lineage-committed cell types. ESCs and iPSCs are an attractive option because they can be expanded in vitro and induced to commit toward different lineages, including myogenic progenitors [64–67]. However, they are still far from clinical use because several aspects still limit their application, such as the ethical problems related to the use of ESCs, the possibility of an immune response against nonautologous and exogenous cells, and the difficulty in the commitment toward muscle cells that must be strongly induced through the use of viral vectors. For all these reasons, we focused our attention directly on tissue specific and possibly autologous progenitors. Human MPCs are able to grow in vitro for several passages, allowing cell expansion for both graft generation and standard cell quality controls [34]. Importantly, with our cell isolation protocol, a population of fibroblasts grows together with muscle cells. This is an important aspect, since other authors demonstrated that fibroblasts improve scaffold regeneration and myogenesis when seeded into the acellular tissue together with muscle cells [8, 68]. In addition, within isolated hMPCs there is a subpopulation of $PAX7^+$ stem cells that allows the culture to self-renew under appropriate conditions [69]. Several studies have shown that, compared with differentiated or committed cells, undifferentiated muscle stem cells are a more potent myogenic cell source, with the ability to engraft and replenish the host satellite cell pool and support future rounds of muscle regeneration [62, 70, 71]. It is therefore believed that for optimal results in engineering muscle tissues, cellular heterogeneity of native muscle should be recreated together with both force-generating, differentiated myofibers, and functioning stem cells to allow further maturation and regeneration prior and after implantation [58]. In our experiments, we demonstrated that hMPCs were able to engraft in the scaffold, proliferate, and repopulate all the layers of the dECM, also interacting with the scaffold and responding to external stimuli. In the device, hMPCs expressing MYF5, the first factor responsible of the skeletal muscle lineage specification in vivo [72], are more sensible to microenvironmental changes, modulating the expression of this marker based on the presence of proliferating or differentiating culture media. Transcription of the skeletal muscle program is then achieved by the subsequent expression of *MYOD* that in turn activates the expression and production of mature skeletal muscle genes and proteins. Indeed, when induced to differentiate, engrafted cells started expressing specific differentiation markers such as ACTA and MYHC. Among all these late myogenic markers, there is also MYH3, a protein exclusively present in developing myofibers [73] that confirms the activation of the entire myogenic program. Moreover, the 3D construct demonstrated to be functioning in vitro and with metabolic active myotubes inside the dECM, a mandatory feature to define a recellularized scaffold as a tissue-like construct.

The engineered muscle must be able also to respond physiologically to damage and remodeling. When we damaged the scaffold with Ctx, mimicking the injury classically used in vivo to stimulate muscle regeneration, $PAX7^+$ engrafted cells increased in number and then generated a population of committed cells that fused together forming new myofibers, suggesting that seeded stem cells were able to recreate a well-structured and organized tissue. Most importantly, they were able to regenerate the stem cell niche, as demonstrated by the increased expression of *LAMA1* and the production of fibronectin which, upon activation of $PAX7^+$ cells by means of a Ctx injury, are indicative of the stem niche remodeling and fundamental events in the mechanism of self-renewal maintenance [46, 47].

The possibility to generate a functional skeletal muscle graft in vitro opens new therapeutic options for the treatment of several defects that require muscle replenishment or substitution. Although decellularized matrices can promote regeneration for volumetric skeletal muscle loss [7, 8], they are associated to high failure rate when used to repair large defects [74]. The latter is a big concern in pediatric surgery, where congenital malformations, such as CDH, do not have a standardized and definitive techniques for defect repair [75, 76]. Hence, the development of a tissue engineered construct combining autologous MPCs from pediatric specimens with a storable biological scaffold deprived of antigenic response, would represent a clinically attractive option for patient-specific therapies. Furthermore, in vivo studies will investigate the efficacy of this muscle construct in the repair of diaphragmatic hernia, especially considering the interaction between seeded and resident cells and the ability to attract vessels and trigger innervation to the site of regeneration. At the same time, such skeletal muscle device could be used in vitro for drug testing and screening, since it could be assimilated to a viable and functional skeletal muscle tissue obtained from specific patients for which tailored therapeutic drugs and dosage are desirable. Furthermore, experiments are needed to test different possible culture conditions (e.g., oxygen tension, mechanical stimuli, dynamic culture) and to optimize cell engraftment, adding, and implementing the recellularization with other important cell types such as macrophages, endothelial, and neural cells, to obtain a more complete in vitro xenograft for possible preclinical and clinical applications.

Conclusion

In the present work, a storable and ready-to-use dECM was used as cell support to generate a self-renewing skeletal muscle construct, as a combination of a mouse-derived ECM and human progenitor cells. We believe that this work represents a step forward toward the generation of tissue engineering xenograft for skeletal muscle clinical applications. As previously demonstrated for the trachea [12], we believe tissue engineered skeletal muscle could be beneficial for the treatment of CDH.

Acknowledgments

This work was supported by Fondazione Istituto di Ricerca Pediatrica Città della Speranza, project number 13/04, by project Fondazione Cariparo-IRP 2013–2016 and Fondazione Cariparo-IRP 2016–2018. M.P. is funded by University of Padova, grant number GRIC15AIPF, Assegno di Ricerca Senior. P.D.C. is supported by the NIHR. All research at Great Ormond Street Hospital NHS Foundation Trust and UCL Great Ormond Street Institute of Child Health is made possible by the NIHR Great Ormond Street Hospital Biomedical Research Centre. The views expressed are those of the author(s) and not

necessarily those of the NHS, the NIHR, or the Department of Health.

Author Contributions

C.T.: conception and design, collection and assembling of the data, data analysis and interpretation, manuscript writing; M.E.A.F., P.C., A.C., E.C., D.B., F.B., F.C., E.B.: collection and assembling of the data; E.M., C.F.: collection and assembling of the data, data analysis and interpretation; P.P.: data analysis and interpretation, financial support; L.U., A.M., P.D.C., M. Pozzobon: data analysis and interpretation; C.B. and L.L.: provision of study material or patients; M. Piccoli: conception and design, data analysis and interpretation, manuscript writing.

Disclosure of Potential Conflicts of Interest

F.C., U.L., P. Michela, and P. Martina are coinventors of Italian Patent number 0001422436 entitled "Matrice acellulare per ricostruzione in vivo di muscolo scheletrico." L.L. is coinventor of Patent number MI2008A001316 entitled "Frazione piastrinica derivante da sangue placentare/Platelet fraction derived from placental blood." The other authors indicated no potential conflicts of interest.

Data Availability Statement

The data that support the findings of this study are available from the corresponding author upon reasonable request.

References

1 Joshi SB, Sen S, Chacko J et al. Abdominal muscle flap repair for large defects of the diaphragm. Pediatr Surg Int 2005;21:677–680.

2 Lally KP, Cheu HW, Vazquez WD. Prosthetic diaphragm reconstruction in the growing animal. J Pediatr Surg 1993;28:45–47.

3 Lee SL, Poulos ND, Greenholz SK. Staged reconstruction of large congenital diaphragmatic defects with synthetic patch followed by reverse latissimus dorsi muscle. J Pediatr Surg 2002;37:367–370.

4 Sydorak RM, Hoffman W, Lee H et al. Reversed latissimus dorsi muscle flap for repair of recurrent congenital diaphragmatic hernia. J Pediatr Surg 2003;38:296–300.

5 Fishman JM, Lowdell MW, Urbani L et al. Immunomodulatory effect of a decellularized skeletal muscle scaffold in a discordant xenotransplantation model. Proc Natl Acad Sci USA 2013;110:14360–14365.

6 Fuoco C, Rizzi R, Biondo A et al. In vivo generation of a mature and functional artificial skeletal muscle. EMBO Mol Med 2015;7:411–422.

7 Sicari BM, Dearth CL, Badylak SF. Tissue engineering and regenerative medicine approaches to enhance the functional response to skeletal muscle injury. Anat Rec 2014;297:51–64.

8 Urciuolo A, Urbani L, Perin S et al. Decellularised skeletal muscles allow functional muscle regeneration by promoting host cell migration. Sci Rep 2018;8:8398.

9 Orabi H, Bouhout S, Morissette A et al. Tissue engineering of urinary bladder and urethra: Advances from bench to patients. Sci World J 2013;2013:154564.

10 Atala A, Bauer SB, Soker S et al. Tissue-engineered autologous bladders for patients needing cystoplasty. Lancet 2006;367:1241–1246.

11 Raya-Rivera AM, Esquiliano D, Fierro-Pastrana R et al. Tissue-engineered autologous vaginal organs in patients: A pilot cohort study. Lancet 2014;384:329–336.

12 Elliott MJ, De Coppi P, Speggiorin S et al. Stem-cell-based, tissue engineered tracheal replacement in a child: A 2-year follow-up study. Lancet 2012;380:994–1000.

13 Atluri P, Trubelja A, Fairman AS et al. Normalization of postinfarct biomechanics using a novel tissue-engineered angiogenic construct. Circulation 2013;128:S95–S104.

14 Guyette JP, Charest JM, Mills RW et al. Bioengineering human myocardium on native extracellular matrix. Circ Res 2016;118:56–72.

15 Wainwright DJ. Use of an acellular allograft dermal matrix (AlloDerm) in the management of full-thickness burns. Burns 1995;21:243–248.

16 De Troyer A, Estenne M. Functional anatomy of the respiratory muscles. Clin Chest Med 1988;9:175–193.

17 Rowley KL, Mantilla CB, Sieck GC. Respiratory muscle plasticity. Respir Physiol Neurobiol 2005;147:235–251.

18 Abu-Hijleh MF, Habbal OA, Moqattash ST. The role of the diaphragm in lymphatic absorption from the peritoneal cavity. J Anat 1995;186:453–467.

19 De Troyer A, Sampson M, Sigrist S et al. The diaphragm: Two muscles. Science 1981;213:237–238.

20 Loukas M, Aqueelah H. Musculocutaneous and median nerve connections within, proximal and distal to the coracobrachialis muscle. Folia Morphol 2005;64:101–108.

21 Martin EC, Bazzy AR, Gandhi MR et al. An investigation into the venous drainage of the diaphragm of the sheep. Invest Radiol 1983;18:272–274.

22 Mittal RK. The crural diaphragm, an external lower esophageal sphincter: A definitive study. Gastroenterology 1993;105:1565–1567.

23 Stuelsatz P, Keire P, Almuly R et al. A contemporary atlas of the mouse diaphragm: Myogenicity, vascularity, and the Pax3 connection. J Histochem Cytochem 2012;60:638–657.

24 Atkinson JB, Poon MW. ECMO and the management of congenital diaphragmatic hernia with large diaphragmatic defects requiring a prosthetic patch. J Pediatr Surg 1992;27:754–756.

25 Clark RH, Hardin WD Jr, Hirschl RB et al. Current surgical management of congenital diaphragmatic hernia: A report from the Congenital Diaphragmatic Hernia Study Group. J Pediatr Surg 1998;33:1004–1009.

26 Grethel EJ, Cortes RA, Wagner AJ et al. Prosthetic patches for congenital diaphragmatic hernia repair: Surgisis vs Gore-Tex. J Pediatr Surg 2006;41:29–33.

27 Lally KP, Paranka MS, Roden J et al. Congenital diaphragmatic hernia. Stabilization and repair on ECMO. Ann Surg 1992;216:569–573.

28 Moss RL, Chen CM, Harrison MR. Prosthetic patch durability in congenital diaphragmatic hernia: A long-term follow-up study. J Pediatr Surg 2001;36:152–154.

29 Sandoval JA, Lou D, Engum SA et al. The whole truth: Comparative analysis of diaphragmatic hernia repair using 4-ply vs 8-ply small intestinal submucosa in a growing animal model. J Pediatr Surg 2006;41:518–523.

30 Keane TJ, Badylak SF. The host response to allogeneic and xenogeneic biological scaffold materials. J Tissue Eng Regen Med 2015;9:504–511.

31 Piccoli M, Urbani L, Alvarez-Fallas ME et al. Improvement of diaphragmatic performance through orthotopic application of decellularized extracellular matrix patch. Biomaterials 2016;74:245–255.

32 Alvarez Fallas ME, Piccoli M, Franzin C et al. Decellularized diaphragmatic muscle drives a constructive angiogenic response in vivo. Int J Mol Sci 2018;19:1329–1338.

33 Jank BJ, Xiong L, Moser PT et al. Engineered composite tissue as a bioartificial limb graft. Biomaterials 2015;61:246–256.

34 Franzin C, Piccoli M, Urbani L et al. Isolation and expansion of muscle precursor cells from human skeletal muscle biopsies. Methods Mol Biol 2016;1516:195–204.

35 Uezumi A, Kasai T, Tsuchida K. Identification, isolation, and characterization of mesenchymal progenitors in mouse and human skeletal muscle. Methods Mol Biol 2016;1460:241–253.

36 Skuk D, Goulet M, Tremblay JP. Preservation of muscle spindles in a 27-year-old Duchenne muscular dystrophy patient: Importance for regenerative medicine strategies. Muscle Nerve 2010;41:729–730.

37 Takahashi H, Shimizu T, Nakayama M et al. The use of anisotropic cell sheets to control orientation during the self-organization of 3D muscle tissue. Biomaterials 2013;34:7372–7380.

38 Scarda A, Franzin C, Milan G et al. Increased adipogenic conversion of muscle satellite cells in obese Zucker rats. Int J Obes 2010;34:1319–1327.

39 van der Velden JL, Schols AM, Willems J et al. Glycogen synthase kinase 3 suppresses

myogenic differentiation through negative regulation of NFATc3. J Biol Chem 2008;283:358–366.

40 Parazzi V, Lazzari L, Rebulla P. Platelet gel from cord blood: A novel tool for tissue engineering. Platelets 2010;21:549–554.

41 Juhas M, Engelmayr GC Jr, Fontanella AN et al. Biomimetic engineered muscle with capacity for vascular integration and functional maturation in vivo. Proc Natl Acad Sci USA 2014;111:5508–5513.

42 Capkovic KL, Stevenson S, Johnson MC et al. Neural cell adhesion molecule (NCAM) marks adult myogenic cells committed to differentiation. Exp Cell Res 2008;314:1553–1565.

43 Pisani DF, Dechesne CA, Sacconi S et al. Isolation of a highly myogenic CD34-negative subset of human skeletal muscle cells free of adipogenic potential. Stem Cells 2010;28: 753–764.

44 Longo V, Rebulla P, Pupella S et al. Proteomic characterization of platelet gel releasate from adult peripheral and cord blood. Proteomics Clin Appl 2016;10:870–882.

45 Parazzi V, Lavazza C, Boldrin V et al. Extensive characterization of platelet gel releasate from cord blood in regenerative medicine. Cell Transplant 2015;24:2573–2584.

46 Rayagiri SS, Ranaldi D, Raven A et al. Basal lamina remodeling at the skeletal muscle stem cell niche mediates stem cell self-renewal. Nat Commun 2018;9:1075.

47 Bentzinger CF, Wang YX, von Maltzahn J et al. Fibronectin regulates Wnt7a signaling and satellite cell expansion. Cell Stem Cell 2013;12: 75–87.

48 Cloonan AJ, O'Donnell MR, Lee WT et al. Spherical indentation of free-standing acellular extracellular matrix membranes. Acta Biomater 2012;8:262–273.

49 Freytes DO, Tullius RS, Badylak SF. Effect of storage upon material properties of lyophilized porcine extracellular matrix derived from the urinary bladder. J Biomed Mater Res B Appl Biomater 2006;78:327–333.

50 Whitson BA, Cheng BC, Kokini K et al. Multilaminate resorbable biomedical device under biaxial loading. J Biomed Mater Res 1998;43:277–281.

51 Urbani L, Maghsoudlou P, Milan A et al. Long-term cryopreservation of decellularised oesophagi for tissue engineering clinical application. PLoS One 2017;12:e0179341.

52 Gouveia BG, Rijo P, Goncalo TS et al. Good manufacturing practices for medicinal products for human use. J Pharm Bioallied Sci 2015;7:87–96.

53 Schuurman HJ. Regulatory aspects of clinical xenotransplantation. Int J Surg 2015; 23:312–321.

54 Turner NJ, Yates AJ Jr, Weber DJ et al. Xenogeneic extracellular matrix as an inductive scaffold for regeneration of a functioning musculotendinous junction. Tissue Eng Part A 2010;16:3309–3317.

55 Sicari BM, Agrawal V, Siu BF et al. A murine model of volumetric muscle loss and a regenerative medicine approach for tissue replacement. Tissue Eng Part A 2012;18:1941–1948.

56 Turner NJ, Badylak JS, Weber DJ et al. Biologic scaffold remodeling in a dog model of complex musculoskeletal injury. J Surg Res 2012;176:490–502.

57 Reing JE, Brown BN, Daly KA et al. The effects of processing methods upon mechanical and biologic properties of porcine dermal extracellular matrix scaffolds. Biomaterials 2010;31: 8626–8633.

58 Quarta M, Cromie M, Chacon R et al. Bioengineered constructs combined with exercise enhance stem cell-mediated treatment of volumetric muscle loss. Nat Commun 2017;8: 15613.

59 Bian W, Bursac N. Engineered skeletal muscle tissue networks with controllable architecture. Biomaterials 2009;30:1401–1412.

60 Cittadella Vigodarzere G, Mantero S. Skeletal muscle tissue engineering: Strategies for volumetric constructs. Front Physiol 2014; 5:362.

61 Koning M, Harmsen MC, van Luyn MJ et al. Current opportunities and challenges in skeletal muscle tissue engineering. J Tissue Eng Regen Med 2009;3:407–415.

62 Rossi CA, Flaibani M, Blaauw B et al. In vivo tissue engineering of functional skeletal muscle by freshly isolated satellite cells embedded in a photopolymerizable hydrogel. FASEB J 2011;25:2296–2304.

63 Conconi MT, Bellini S, Teoli D et al. In vitro and in vivo evaluation of acellular diaphragmatic matrices seeded with muscle precursors cells and coated with VEGF silica gels to repair muscle defect of the diaphragm. J Biomed Mater Res A 2009;89:304–316.

64 Chal J, Oginuma M, Al Tanoury Z et al. Differentiation of pluripotent stem cells to muscle fiber to model Duchenne muscular dystrophy. Nat Biotechnol 2015;33:962–969.

65 Darabi R, Arpke RW, Irion S et al. Human ES- and iPS-derived myogenic progenitors restore DYSTROPHIN and improve contractility upon transplantation in dystrophic mice. Cell Stem Cell 2012;10:610–619.

66 Rao L, Qian Y, Khodabukus A et al. Engineering human pluripotent stem cells into a functional skeletal muscle tissue. Nat Commun 2018;9:126.

67 Shelton M, Metz J, Liu J et al. Derivation and expansion of PAX7-positive muscle progenitors from human and mouse embryonic stem cells. Stem Cell Rep 2014;3:516–529.

68 Perniconi B, Costa A, Aulino P et al. The pro-myogenic environment provided by whole organ scale acellular scaffolds from skeletal muscle. Biomaterials 2011;32:7870–7882.

69 Lepper C, Conway SJ, Fan CM. Adult satellite cells and embryonic muscle progenitors have distinct genetic requirements. Nature 2009;460: 627–631.

70 Montarras D, Morgan J, Collins C et al. Direct isolation of satellite cells for skeletal muscle regeneration. Science 2005;309:2064–2067.

71 Sacco A, Doyonnas R, Kraft P et al. Self-renewal and expansion of single transplanted muscle stem cells. Nature 2008;456:502–506.

72 Conerly ML, Yao Z, Zhong JW et al. Distinct activities of Myf5 and MyoD indicate separate roles in skeletal muscle lineage specification and differentiation. Dev Cell 2016; 36:375–385.

73 Schiaffino S, Rossi AC, Smerdu V et al. Developmental myosins: Expression patterns and functional significance. Skelet Muscle 2015;5:22.

74 Bekdash B, Singh B, Lakhoo K. Recurrent late complications following congenital diaphragmatic hernia repair with prosthetic patches: A case series. J Med Case Rep 2009; 3:7237.

75 Basile F, Biondi A, Donati M. Surgical approach to abdominal wall defects: History and new trends. Int J Surg 2013;11:S20–S23.

76 Puligandla PS, Grabowski J, Austin M et al. Management of congenital diaphragmatic hernia: A systematic review from the APSA outcomes and evidence based practice committee. J Pediatr Surg 2015;50:1958–1970.

See www.StemCellsTM.com for supporting information available online.